Review

A Review on Advanced AFM and SKPFM Data Analytics for Quantitative Nanoscale Corrosion Characterization

Mohammad Reza Attar and Ali Davoodi *,†

Posted Date: 23 September 2025

doi: 10.20944/preprints202509.1851.v1

Keywords: corrosion mechanisms; AFM; SKPFM; advanced data analysis; surface heterogeneity

 doi:10.20944/preprints202509.1851.v1

Review

A Review on Advanced AFM and SKPFM Data Analytics for Quantitative Nanoscale Corrosion Characterization

Mohammad Reza Attar and Ali Davoodi *,†

Department of Materials and Metallurgical Engineering, Ferdowsi University of Mashhad, Mashhad, Iran

* Correspondence: davoodiali@gmail.com

† Current Address: Yacht, High Tech Campus 32, 5656 AE Eindhoven, The Netherlands.

Abstract

Corrosion is a complex, surface-initiated process that demands nanoscale, real-time characterization to understand its initiation and propagation. Atomic Force Microscopy (AFM) and Scanning Kelvin Probe Force Microscopy (SKPFM) have emerged as powerful tools in corrosion science, enabling high-resolution imaging and electrochemical mapping under realistic conditions. This review, inspired by pioneering work at KTH by Professors Christofer Leygraf and Jinshan Pan, highlights advanced analytical strategies that extend the capabilities of AFM and SKPFM beyond traditional line-profile analysis. Techniques such as power spectral density (PSD) analysis, multimodal Gaussian histogram fitting, statistical roughness quantification, and deconvolution methods are discussed in the context of case studies on aluminum alloys, stainless steels, magnesium alloys, biomedical implants, and protective coatings. By integrating in-situ imaging, electrochemical mapping, and statistical data processing, these approaches provide deeper insights into localized corrosion, micro-galvanic coupling, and surface reactivity. Future directions include coupling AFM-based methods with high-speed imaging, machine learning, and spectro-electrochemical techniques to accelerate the development of corrosion-resistant materials and predictive diagnostics.

Keywords: corrosion mechanisms; AFM; SKPFM; advanced data analysis; surface heterogeneity

1. Introduction

Corrosion, a surface-driven process, poses significant challenges across industries, from infrastructure to biomedical applications. Generally, corrosion initiates at the metal–electrolyte interface, making surface tracking and real-time monitoring critical for understanding its mechanisms. While attempt to perform in-situ transmission electron microscopy (TEM) are growing fast (despite the challenges), traditional ex-situ techniques—optical microscopy, scanning electron microscopy (SEM), TEM, and spectroscopy—provide post-exposure snapshots but lack the ability to capture dynamic corrosion processes in aqueous environments. Additionally, transferring samples during ex-situ characterization introduces artifacts that hinder accurate identification of corrosion initiation sites and may alter the composition of corrosion products, potentially misleading the interpretation of corrosion mechanisms. In-situ visualization of active corrosion remains a key research goal, as it enables direct observation of surface reactions and electrochemical heterogeneity. Atomic Force Microscopy (AFM), a subset of scanning probe microscopy (SPM), addresses these challenges with its nanoscale resolution and ability to operate in liquid environments. AFM tracks topographical changes and electrochemical activity at the metal–electrolyte interface, offering insights unattainable by ex-situ methods. This becomes even more powerful when AFM is combined with complementary characterization techniques.

This review, building on over a decade of corrosion and AFM expertise at KTH with collaborators Christofer Leygraf and Jinshan Pan, synthesizes key findings from in-situ AFM studies

 doi:10.20944/preprints202509.1851.v1

and advanced data analysis. It highlights mechanistic insights into corrosion initiation and propagation, showcases applications across diverse materials, and proposes future directions for integrating AFM with emerging technologies to advance corrosion research. AFM's high-resolution topographical imaging has proven invaluable in tracking the early morphological changes that accompany corrosion processes. Line profile analyses of surfaces revealed characteristic trenching patterns and pit nucleation around reactive intermetallic particles (IMPs), offering direct visual and quantitative evidence of localized material loss in aluminum alloys.

The application of AFM in corrosion science has significantly enhanced the mechanistic understanding of localized corrosion, particularly in aluminum alloys such as EN AW-3003. J. Pan and C. Leygraf at KTH studied the effect of intermetallic particles on localized corrosion of aluminum alloys using ex-situ SKPFM and in-situ AFM [1-7]. The dual approach allowed direct correlation of Volta potential distributions with IMP corrosion activity, especially in chloride environments. As illustrated in Figure 1a-c SKPFM analyses revealed that larger constituent IMPs—typically Fe- and Si-rich phases such as Al(Mn,Fe)Si (identified by SEM-EDS analysis)—exhibited significantly higher Volta potentials than the aluminum matrix, acting as cathodic sites. In contrast, nanoscale dispersoids (<0.5 μm), such as $Al_{12}Mn_3Si$, showed negligible Volta potential differences and minimal electrochemical reactivity. In-situ AFM observations confirmed that corrosion initiated at the boundaries of micrometer-sized IMPs through micro-galvanic interactions, leading to localized anodic dissolution and trench formation. The boundary regions, where Volta potential minima were observed, were identified as critical weak points for corrosion initiation [4].

In another study, Örnek et al. [8] conducted several investigations on grade 2205 DSS to understand its corrosion behavior. In 2015, they explored how Volta potential differences between ferrite and austenite phases—measured by SKPFM—correlated with strain localization, revealing potential differences of 70–90 mV that drove selective ferrite dissolution in annealed DSS, while cold-rolled DSS showed localized pitting in austenite linked to strain-induced potential hotspots (Figure 1d-f). The following year, they combined EBSD and SKPFM to characterize microstructural features in aged DSS, identifying Cr_2N, r-phase, and v-phase as cathodic sites that promoted ferrite corrosion [9]. In 2019, further investigations by Rahimi et al. [10] using SKPFM and STEM-EDS confirmed the higher nobility of ferrite, with a Volta potential difference of approximately $\Delta V \approx 50\, mV$ due to enrichment in Mo, W, and Cr. Mott-Schottky analysis also revealed the presence of p- and n-type layers within the passive film on the different phases.

 doi:10.20944/preprints202509.1851.v1

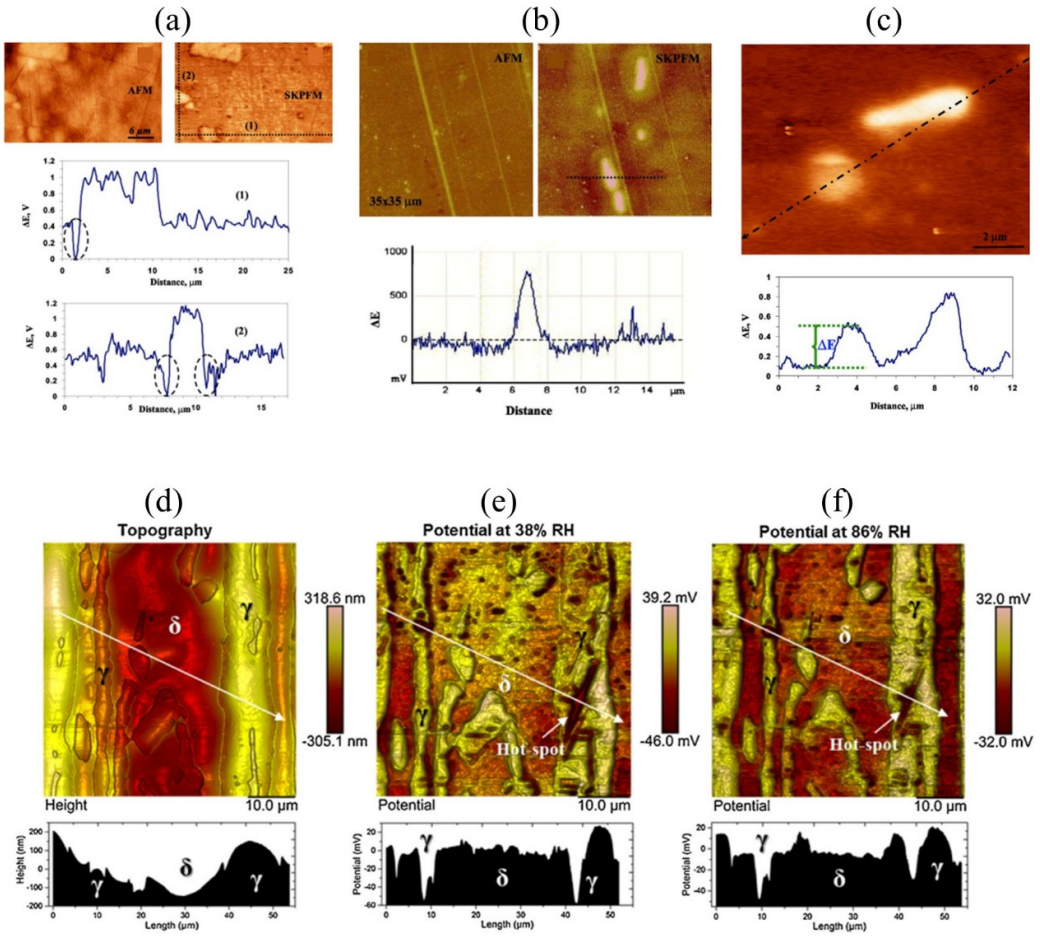

Figure 1. Representative AFM and SKPFM data illustrating topography and Volta potential distribution on metallic surfaces under different preparation and imaging conditions. (a) Topography and Volta potential images of a polished EN AW-3003 aluminum alloy surface obtained in one-pass mode, together with Volta potential line profiles across IMP–matrix boundaries. (b) Topography and Volta potential images of an ultramicrotomed EN AW-3003 surface imaged in two-pass mode, including a corresponding Volta potential line profile; topographical variation spans 50 nm. (c) Volta potential image and line profile acquired in one-pass mode from a polished EN AW-3003 surface, showing Volta potential differences between IMPs, dispersoids, and the matrix [4]. (d) SKPFM topography of 40% cold-rolled 2205 duplex stainless steel. (e) Mathematically inverted Volta potential map of the same sample recorded at 38% RH, highlighting local potential hot-spots. (f) Volta potential map at 86% RH, confirming the persistence of local hot-spots as corrosion-active sites. Potential maps (d–f) were processed using first-order flattening; thus, values are relative only [8].

A recent study examined how grain boundary chemistry and precipitate structure affect intergranular corrosion in Cu- and Zn-doped Al-Mg-Si alloys, with STEM-EDS showing Zn segregation at grain boundaries that enhanced corrosion susceptibility [11]. Statistical AFM analysis was also suggested to quantify precipitate-driven corrosion more precisely, providing deeper mechanistic insights into the impact of impurities in recycled alloys.

Research on martensitic stainless steels processed by quenching and partitioning employed SKPFM and SECM to detect pit initiation at MnS and TiN inclusions [12]. The researchers observed a Volta potential difference of approximately 40 mV between inclusions and the matrix, which drove selective dissolution at their interfaces, emphasizing the critical role of inclusions in localized corrosion.

Despite these advances, a complete mechanistic picture requires further integration of AFM with complementary techniques. Overall, AFM—especially when integrated with SKPFM—serves not

 doi:10.20944/preprints202509.1851.v1

only as a topographical imaging tool but also as a powerful platform for electrochemical corrosion analysis. Its ability to resolve sub-micrometer activity makes it indispensable for dissecting microstructural influences on corrosion initiation. However, the results remain largely qualitative and highlight the need to refine quantitative descriptors and expand temporal resolution. In other words, conventional AFM analysis—reliant on one-dimensional line profiles—is insufficient for capturing the spatial extent, lateral heterogeneity, or mechanistic details of corrosion. Advanced data analysis techniques—such as power spectral density (PSD), SKPFM, multimodal Gaussian histograms, and statistical roughness quantification—offer a multidimensional perspective, enabling quantitative correlations between microstructure, surface properties, and corrosion behavior. The following section briefly reviews PSD, multimodal Gaussian histograms, and statistical roughness quantification.

2. Advanced AFM and SKPFM Data Analysis Techniques

2.1. Power Spectral Density Analysis

PSD analysis decomposes surface topography into its spatial frequency components, allowing for the identification of dominant roughness scales. It is calculated using the Fourier transform of the surface height variation, as shown below:

$$PSD(k_x k_y) = \left| \frac{1}{L_x L_y} \int_0^{L_x} \int_0^{L_y} h(x,y) e^{-i(k_x x + k_y y)} \, \mathrm{d}y \, \mathrm{d}x \right|^2 \quad (1)$$

where $h(x,y)$ represents the surface height, k_x and k_y are the spatial frequencies in the x and y directions, and L_x and L_y denote the scan dimensions along those axes. The integral performs the two-dimensional Fourier transform of the topographical data. PSD is typically plotted as spectral power (e.g., nm^2/Hz or V^2/Hz) versus spatial frequency ($1/\mu m$). It offers a robust and scale-invariant characterization of roughness, enabling comparison between surfaces with different morphologies or potential distributions. PSD is also relatively insensitive to random noise, enhancing the reliability of surface analysis. Despite these advantages, PSD analysis assumes that the surface features are stationary over the scan area—a condition not always valid for highly heterogeneous corrosion surfaces. Moreover, tip convolution effects and limited spatial resolution can introduce distortions, particularly in the high-frequency range. In corrosion studies, PSD can be employed to monitor changes in roughness due to corrosion progression, such as the emergence of high-frequency components indicative of pitting. It also aids in detecting periodic patterns of corrosion, for example, along grain boundaries or other microstructural features.

2.2. Multimodal Gaussian & Histogram Analysis

AFM and SKPFM data often display complex statistical distributions arising from the presence of different surface features, such as oxides, metal substrate regions, and corrosion products. These variations can be effectively analyzed using histogram-based methods, where the data distribution is fitted with multiple Gaussian functions to extract distinct populations. Given a histogram $p(z)$ of surface heights or potential values, a multimodal Gaussian fit expresses the distribution as a sum of N individual Gaussian components:

$$p(z) = \sum_{i=1}^{N} \frac{A_i}{\sigma_i \sqrt{2\pi}} \exp\left(-\frac{(z-\mu_i)^2}{2\sigma_i^2} \right) \quad (2)$$

In this expression, A_i represents the amplitude of the i-th Gaussian, μ_i is the mean value (e.g., height or potential), and σ_i is the standard deviation, which reflects the degree of variation or heterogeneity within each population. This approach enables the statistical separation of overlapping surface features and provides quantitative insight into the underlying material phases or corrosion products, independent of their spatial distribution. While histogram analysis is straightforward to compute and interpret, it comes with limitations. The method assumes that the distributions are Gaussian in nature, which may not always hold true for complex or irregular corrosion-induced features. Additionally, selecting too many Gaussian components can lead to overfitting, reducing the reliability of the analysis. Histograms inherently lack spatial context, making it difficult to assess the

 doi:10.20944/preprints202509.1851.v1

arrangement or distribution of features across the surface. Therefore, they are often used in conjunction with spatially resolved methods such as PSD analysis. Furthermore, the choice of bin size significantly influences the resolution and sensitivity to noise in the histogram. This technique is particularly useful for quantifying oxide thickness distributions in passive films and identifying localized corrosion features. For instance, the presence of secondary peaks in a histogram may signal the onset of pit formation or the emergence of corrosion products distinct from the base material.

2.3. Convolution & Deconvolution in AFM/SKPFM

AFM and SKPFM images are inherently influenced by the geometry of the probe tip, resulting in a convolution of the true surface features with the tip shape. This leads to image broadening, particularly for sharp or recessed features, which can obscure nanoscale corrosion phenomena. Deconvolution techniques aim to reconstruct the true surface morphology by mathematically compensating for these tip-induced distortions. The image formation process can be described by the convolution model:

$$I(x,y) = S(x,y) * T(x,y) + Noise \quad (3)$$

where $I(x,y)$ is the measured image, $S(x,y)$ is the actual surface topography, $T(x,y)$ is the tip shape function, and the convolution operator $(*)$ accounts for the geometric interaction between the tip and the surface. The noise term represents random measurement errors or instrumental artifacts.

To recover $S(x,y)$, deconvolution methods are employed. One common approach is blind deconvolution, where both the tip shape and the true surface are iteratively estimated without prior knowledge of the tip geometry. Alternatively, Wiener filtering offers a frequency-domain correction technique that incorporates noise suppression and a known or estimated point spread function (PSF) for the system. These methods can significantly improve spatial resolution, allowing detection of submicron corrosion features such as pits, cracks, or fine grain boundary attacks that may otherwise be masked by tip effects. Deconvolution also enhances electrochemical mapping accuracy in techniques such as Amplitude-Modulated SKPFM (ASPFM), where fine potential variations are critical for understanding localized activity. However, deconvolution is sensitive to noise and relies heavily on accurate PSF estimation. Inaccurate modeling of the tip or over-application of the algorithm can lead to image artifacts or the misinterpretation of surface features. Overall, deconvolution techniques are a valuable complement to other analysis methods. When combined with PSD analysis, multimodal Gaussian fitting, and histogram-based interpretation, they form a comprehensive toolkit for nanoscale corrosion evaluation. This integrated approach enables quantitative tracking of surface roughness evolution, statistical differentiation of corrosion phases, and improved resolution of localized degradation features critical for understanding early-stage corrosion mechanisms.

3. Applications of Advanced AFM and SKPFM in Corrosion Science

Advanced AFM and SKPFM have emerged as cornerstone techniques in corrosion science, offering unparalleled insights into the nanoscale electrochemical and topographical characteristics of material surfaces. By employing methods such as PSD, multimodal Gaussian histograms, and statistical roughness quantification, these techniques surpass the limitations of traditional line profile analysis, which provides only one-dimensional data and fails to capture the complex heterogeneity and dynamic electrochemical behavior of corroding surfaces. Advanced AFM and SKPFM enable researchers to map surface potential variations, identify corrosion initiation sites, and correlate microstructural features with corrosion susceptibility across diverse material systems. These methods are often integrated with complementary techniques, such as Scanning Electron Microscopy (SEM), Energy-Dispersive X-ray Spectroscopy (EDS), Electrochemical Impedance Spectroscopy (EIS), and Scanning Electrochemical Microscopy (SECM), to provide a comprehensive understanding of corrosion mechanisms. The following sections categorize these applications into distinct material systems and phenomena, detailing key studies, their methodologies, findings, and the specific

 doi:10.20944/preprints202509.1851.v1

advantages of advanced AFM techniques over conventional line profiles. Each section emphasizes the transformative impact of these methods in advancing corrosion science and material design.

3.1. Dissimilar Metal Welds and Joints

Dissimilar metal welds and joints, such as those combining aluminum, copper, titanium, and steel, are critical in industries like aerospace, automotive, and marine engineering, where they enable the integration of complementary material properties, such as lightweight strength and corrosion resistance. However, the welding process—whether through friction stir welding (FSW), solid-state welding, or other methods—introduces microstructural heterogeneity, including intermetallic compounds (IMCs) and phase boundaries, which often act as galvanic corrosion hotspots. Advanced AFM and SKPFM techniques have been pivotal in characterizing these interfaces, mapping electrochemical activity with nanoscale precision, and providing quantitative data to guide the development of corrosion-resistant welds. By resolving Volta potential differences and roughness variations, these methods reveal the mechanisms driving localized corrosion and inform strategies to mitigate degradation in harsh environments.

Figure 2a presents the AFM and SKPFM results from a multimodal study by Sarvghad-Moghaddam et al. [13] on friction stir welded aluminum–copper joints, which are prone to galvanic corrosion due to the electrochemical potential difference between the two metals. The interfacial regions were comprehensively characterized using SEM-EDS, AFM, SKPFM, and optical microscopy. SKPFM revealed that $CuAl_2$ IMCs exhibited Volta potentials 200–300 mV higher than the Al-rich matrix, identifying them as micro-galvanic sites. Multimodal Gaussian histograms quantified the Volta potential distributions, showing that corrosion preferentially initiated at IMC boundaries where potential differences (ΔV) exceeded 250 mV. Post-immersion in 3.5% NaCl, dynamic electrochemical shifts were observed, with copper becoming anodic due to the formation of a passive oxide layer on titanium, a phenomenon captured by SKPFM's real-time mapping capabilities. The study highlighted the role of microstructural heterogeneity, driven by tool pin and shoulder effects during FSW, in promoting localized corrosion in Al-rich zones adjacent to dispersed Cu particles. This work demonstrated SKPFM's ability to provide spatially resolved electrochemical data, critical for understanding corrosion initiation in complex weld interfaces.

In 2016, Davoodi et al. [14] conducted a comprehensive investigation into the microstructure and corrosion behavior of the interfacial region in dissimilar friction stir welded AA5083 and AA7023 aluminum alloys. This study employed a suite of techniques, including SEM-EDS, optical microscopy, potentiodynamic polarization, EIS, AFM, and SKPFM, to investigate the corrosion behavior of the weld interface. An inhomogeneous borderline rich in Al-Mg-Zn precipitates was identified as a galvanic cell, with SKPFM detecting Volta potential differences of 700–800 mV between AA5083 and AA7023 (Figure 2b). Corrosion initiated at Cu/Si-rich IMPs on the AA7023 side and Al-Mn-Fe particles on the AA5083 side, driven by these significant potential gradients. A follow-up study in 2018 applied PSD and histogram analysis of AFM and SKPFM images to quantitatively assess roughness and electrochemical variations at the AA7023/AA5083 interface [15]. AA5083 exhibited uniform roughness and lower Volta potentials at high spatial frequencies, while AA7023 showed higher roughness and Volta potentials at low frequencies, correlating with corrosion susceptibility at the FSW interface. Gaussian and fast Fourier transform (FFT) analyses provided quantitative insights into the corrosion extent at Al-Mn-Fe particles, highlighting the limitations of line profiles in capturing such complex surface dynamics.

 doi:10.20944/preprints202509.1851.v1

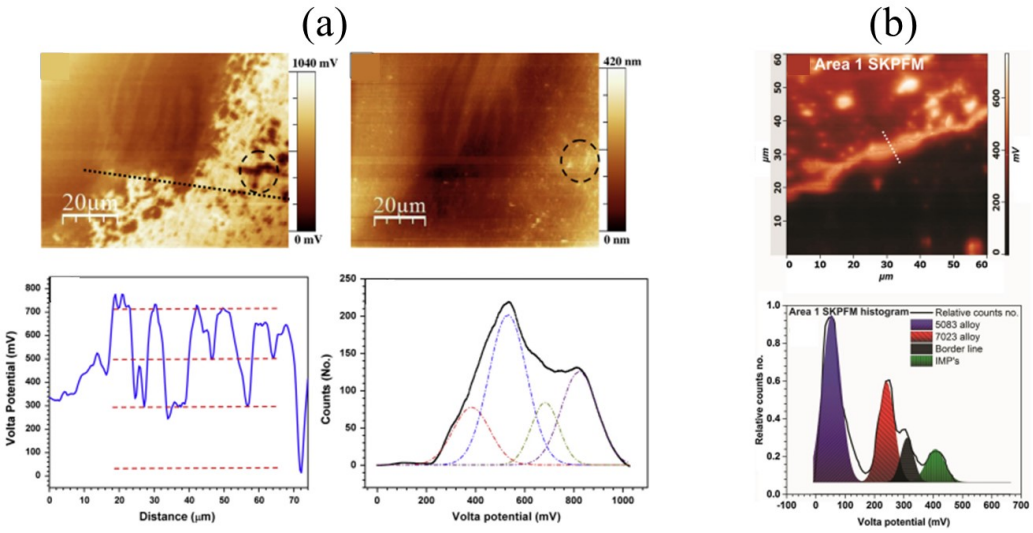

Figure 2. SKPFM and AFM characterization of aluminum alloy interfaces and friction stir welded regions. (a) AFM and SKPFM images of the Al/Cu interface, showing the Volta potential line profile and the corresponding histogram with a fitted quadrumodal Gaussian distribution [13]. (b) SKPFM images of the friction stir welded interfacial region between dissimilar AA5083 and AA7023 alloys, highlighting the potential distribution across the joint. Histogram analysis of the Volta potential shows distinct upper and lower regions corresponding to AA7023 and AA5083, respectively [14].

In 2018, Rahimi et al. [16, 17] conducted a detailed analysis of galvanic behavior in a solid-state welded Ti-Cu bimetal, focusing on how local intermetallic phases influence corrosion initiation. Using SKPFM, the researchers mapped Ti_2Cu, TiCu, and $TiCu_4$ IMCs as anodic sites, revealing Volta potential differences of approximately 400 mV compared to the surrounding matrix. Before immersion in 3.5% NaCl, the Cu side displayed higher nobility, indicating a greater corrosion susceptibility for titanium (Figure 3a). However, after immersion, the development of a passive titanium oxide layer reversed this behavior, rendering copper anodic. Gaussian distribution and FFT analyses were applied to quantify the electrochemical activity in local melted and vortex zones, demonstrating SKPFM's capability to monitor dynamic galvanic interactions. This work emphasized the need to account for both microstructural and electrochemical variables when designing dissimilar metal joints for harsh environments such as marine applications.

Okonkwo et al. [18] conducted a microscale investigation on the galvanic corrosion behavior of low-alloy steel A508 joined with stainless steel 309L/308L weld overlays. Using a combination of optical microscopy, SEM, SVET, and AFM, they identified MnS inclusions within the heat-affected zone (HAZ) as primary sites for pitting initiation. Microstructural transformation in the HAZ—from tempered bainite to a bainite–martensite mixture—was linked to increased corrosion susceptibility. Quantitative analysis through Gaussian distribution and fast Fourier transform (FFT) applied to AFM data allowed for precise assessment of localized corrosion (Figure 3b). In a subsequent study, the same group introduced a novel approach to evaluate how variations in anode/cathode area ratios and microstructural differences influence galvanic corrosion [19]. AFM-PSD results revealed that grain-refined areas and MnS inclusions exhibited the highest electrochemical activity. They further observed that reducing the anode-to-cathode area ratio significantly intensified local corrosion current density, highlighting the critical role of microstructural features in the corrosion behavior of dissimilar welds.

 doi:10.20944/preprints202509.1851.v1

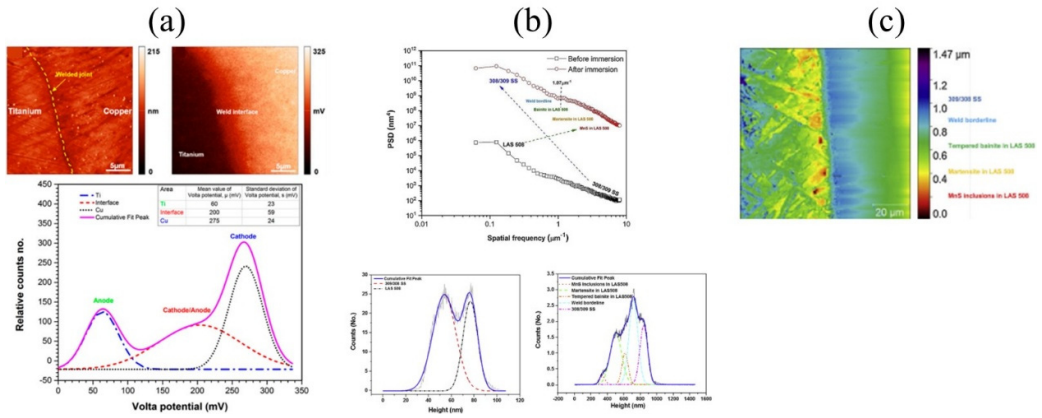

Figure 3. Representative AFM and SKPFM analyses illustrating surface topography and Volta potential characteristics of dissimilar metal interfaces. (a) AFM and SKPFM images of the Ti/Cu weld interface before immersion, with the corresponding histogram of Volta potential differences highlighting regions susceptible to galvanic corrosion [17]. (b) PSD profiles and multi-modal Gaussian histograms derived from AFM topography images before and after immersion, indicating changes in surface roughness and feature distribution due to exposure to a corrosive environment [18]. (c) Rainbow-colored AFM image showing the correlation between surface constituents and topographical features [18].

Compared to traditional line profiles, SKPFM offers several significant advantages for analyzing weld interfaces. First, it enables high-resolution electrochemical mapping by providing spatially resolved Volta potential data. This capability allows for the identification of micro-galvanic sites, such as IMCs and IMPs, and the detection of dynamic electrochemical shifts like nobility inversions—phenomena that line profiles, limited by their one-dimensional and non-electrochemical nature, cannot capture. Second, PSD analysis complements this by offering a comprehensive evaluation of surface roughness in relation to corrosion susceptibility across a range of spatial frequencies. This multi-scale, quantitative insight reveals weld interface heterogeneity far more effectively than the limited topographic information available from line profiles. Finally, in-situ SKPFM facilitates real-time monitoring of electrochemical activity, making it possible to observe transient behaviors such as galvanic polarity shifts and the early stages of corrosion at weld interfaces. These capabilities are critical for improving weld design and enhancing corrosion resistance.

3.2. Biomedical Alloys and Implants

Biomedical alloys, such as titanium (Ti-6Al-4V), cobalt-chromium-molybdenum (CoCrMo), and magnesium (Mg) alloys, are essential for implants and medical devices due to their mechanical strength, biocompatibility, and corrosion resistance. However, their performance in physiological environments is influenced by complex interactions with proteins, electrolytes, and oxidative species, which can accelerate corrosion and biodegradation. Advanced AFM and SKPFM techniques have been critical in studying these interactions at the nanoscale, providing detailed insights into protein adsorption, passive film stability, and electrochemical dynamics. These methods enable researchers to correlate surface potential changes and topographic features with corrosion behavior, informing the design of durable and biocompatible implants.

In 2015, Nakhaie et al. [20] conducted a comprehensive investigation into how cold plastic deformation affects the passive behavior of Ti-6Al-4V alloy, utilizing both electrochemical methods and localized surface probing techniques. Using potentiodynamic polarization, Mott-Schottky analysis, AFM, and SKPFM, the study found that cold working increased passive current density and introduced defects into the passive film, correlating with increased bulk crystal defects. SKPFM revealed that the α-phase had a Volta potential 38.6 mV lower than the β-phase, making it more vulnerable to corrosion in aggressive environments (Figure 4). Mott-Schottky analysis confirmed the n-type semiconducting behavior of the passive layer and showed that higher film formation

 doi:10.20944/preprints202509.1851.v1

potentials reduced donor density, mitigating some effects of cold work. In 2021, Rahimi et al. [21] explored how exposure to hydrogen peroxide influences the adsorption behavior of bovine serum albumin on Ti-6Al-4V alloy surfaces, using scanning Kelvin probe force microscopy to assess the electrochemical implications. SKPFM showed that hydrogen peroxide (H_2O_2) disrupted bovine serum albumin (BSA) adsorption, leading to a thinner, discontinuous protein layer and a reduced surface potential, which increased corrosion rates. Another 2021 study explored TiO_2 nanotube growth on Ti-6Al-4V, revealing faster oxide formation on β-phases due to higher Al/V content [22]. AFM quantified morphological differences through statistical roughness analysis, highlighting the role of phase composition in oxide growth kinetics.

In 2022, Rahimi et al. [23] examined the effect of albumin protein adsorption on the localized corrosion behavior of CoCrMo implant alloy, utilizing advanced surface characterization techniques to reveal electrochemical changes at the microscale. SKPFM revealed that BSA adsorption formed clusters with lower surface potentials, accelerating corrosion at protein/substrate interfaces. Increasing BSA concentrations from 0.5 to 2 g/L and applying overpotentials of +300 mV (vs. Ag/AgCl) enhanced protein coverage and corrosion rates, as confirmed by field emission SEM. Mott-Schottky analysis indicated increased space charge capacitance in the presence of BSA, facilitating metal ion release. This study highlighted SKPFM's ability to map nanoscale electrochemical interactions at protein-metal interfaces, critical for understanding corrosion in biomedical implants exposed to physiological media.

In 2024, Imani et al. [24] explored the early-stage in vitro biodegradation behavior of WE43 magnesium alloy in simulated body fluids, using AFM and SKPFM to assess the impact of albumin protein on surface degradation and electrochemical response. SKPFM detected a 10–20 nm BSA nanolayer with aggregated and fibrillar morphology in Hanks' solution, reducing surface potential by 52 mV and increasing biodegradation rates. In contrast, BSA in NaCl solution inhibited corrosion, increasing impedance from 49 to 97 $\Omega \cdot cm^2$ and reducing electrochemical current noise (ECN). Statistical roughness analysis quantified film morphology, revealing a dual-mode biodegradation behavior influenced by electrolyte composition. This study underscored the role of protein-electrolyte interactions in modulating Mg alloy degradation, critical for orthopedic and cardiovascular applications.

 doi:10.20944/preprints202509.1851.v1

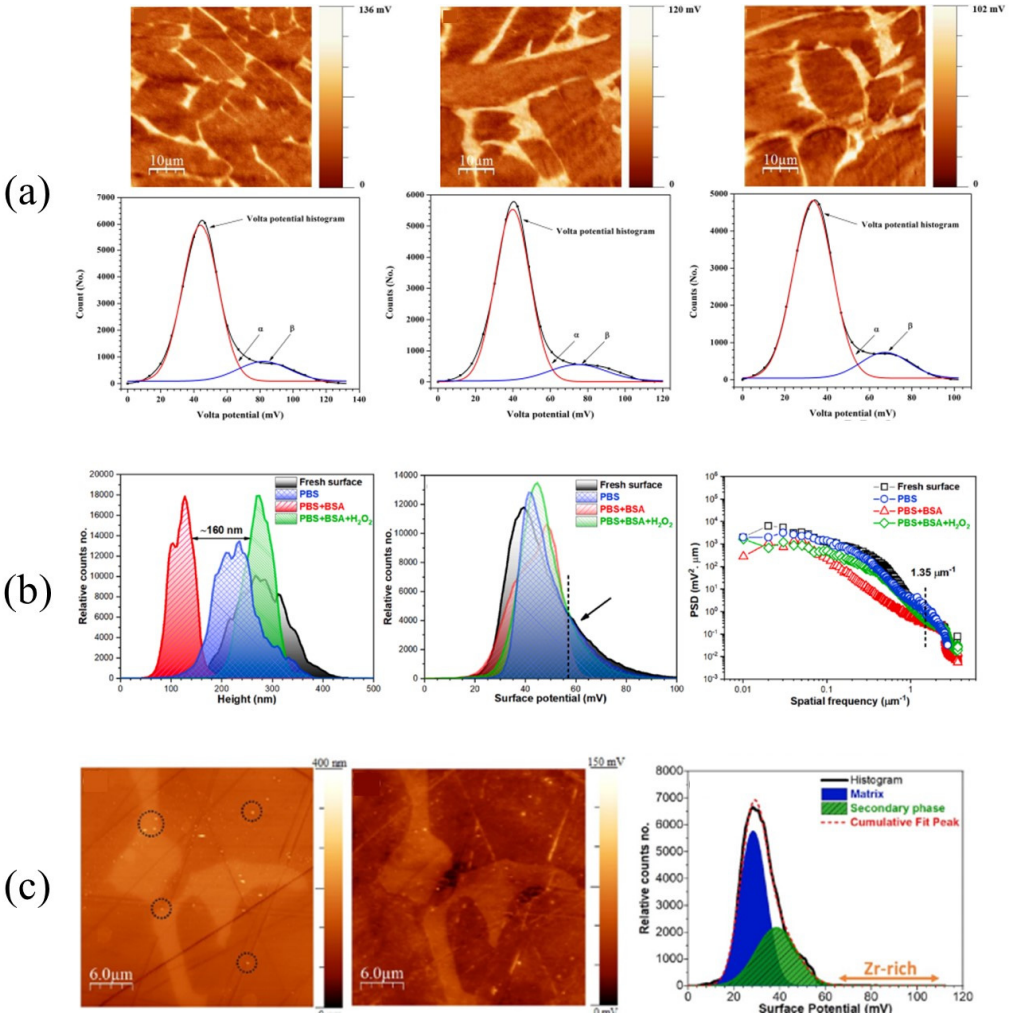

Figure 4. (a) Volta potential maps and corresponding deconvoluted histograms of Ti-6Al-4V alloy under different deformation states (solution treated, 2% cold worked, and 5% cold worked), showing phase-dependent potential distributions [20]. (b) Surface topography, potential histograms, and 1D PSD analysis of Ti-6Al-4V alloy under different surface conditions [21]. (c) AFM and SKPFM images of an as-polished Mg-based alloy with the associated surface potential distribution histogram, highlighting variations linked to microstructural features [25].

The use of SKPFM in conjunction with AFM topography, Mott-Schottky analysis, and SEM offers a robust approach for understanding surface interactions in physiological environments. SKPFM enables high-resolution mapping of potential changes induced by protein adsorption, revealing electrochemical dynamics at the nanoscale that traditional line profiles cannot capture. The integration of multiple characterization techniques provides a multidimensional view of the surface, linking morphological features with corrosion and biodegradation mechanisms. Furthermore, roughness metrics and power spectral density analysis deliver quantitative assessments of topographic variations, allowing for detailed evaluation of protein film formation and passive layer integrity.

3.3. Protective Coatings and Superhydrophobic Surfaces

Protective coatings, including superhydrophobic surfaces and thin dense chromium (TDC) coatings, are designed to enhance corrosion resistance by modifying surface morphology and electrochemical properties. These coatings are critical in applications ranging from marine engineering to industrial machinery, where exposure to aggressive environments like chloride

 doi:10.20944/preprints202509.1851.v1

solutions is common. Advanced AFM and SKPFM techniques have been instrumental in optimizing coating design by quantifying nanoscale roughness, identifying defect-driven galvanic cells, and correlating surface properties with corrosion performance. These methods provide detailed insights into the interplay between microstructure, surface potential, and corrosion resistance, guiding the development of durable coatings.

Rahimi et al. [26, 27] investigated how modifying the surface morphology of electrodeposited superhydrophobic nickel coatings can enhance corrosion resistance (Figure 5). Using a combination of AFM, SEM-EDS, and electrochemical measurements, the study explored the relationship between surface structure and protective performance, providing valuable insights into the design of corrosion-resistant coatings. AFM revealed that boric acid promoted the formation of micro-nano cone structures, achieving contact angles >150° and reducing corrosion current by a factor of 10. PSD and histogram analysis confirmed screw dislocation-driven growth, with a contact angle of 156° correlating with enhanced hydrophobicity. A related study examined the behavior of water and saline droplets during icing and melting cycles on superhydrophobic surfaces [28]. The findings demonstrated that superhydrophobic nickel films significantly delayed freezing—up to 110 minutes—compared to just 34 minutes for bright nickel surfaces. This enhanced performance was attributed to the broader roughness distribution of the superhydrophobic films across all spatial frequencies. SEM-EDS complemented AFM by visualizing structural changes and organic contaminants contributing to hydrophobicity.

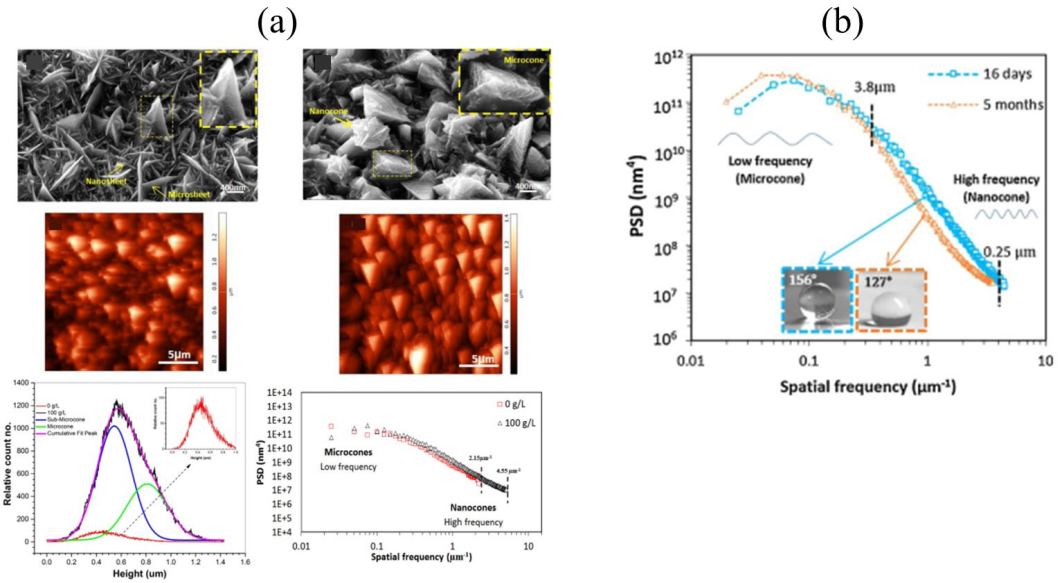

Figure 5. (a) SEM and AFM images of nickel micro–nanostructures deposited with and without H_3BO_3, along with corresponding histogram and PSD plots derived from AFM data [27]. (b) PSD versus spatial frequency for nickel electrodeposited coatings containing 200 g L^{-1} H_3BO_3 after 16 days and 5 months of air exposure, calculated from AFM topography images [26].

The influence of an inorganic corrosion inhibitor on the electrochemical behavior of superhydrophobic micro/nano-structured Ni films in 3.5% NaCl solution was investigated by Noorbakhsh-Nezhad et al. [29]. AFM quantified a root-mean-square (RMS) roughness of 14.4 nm and skewness of 0.21, correlating with 80% corrosion inhibition efficiency when 0.1 M sodium molybdate was used as an inhibitor. EIS confirmed that the films acted as non-ideal capacitors, enhancing durability in aggressive NaCl solutions. The study highlighted the role of surface morphology in improving corrosion resistance, with AFM providing detailed topographic data.

Attar et al. [30, 31] highlight the central role of AFM in linking surface topography to performance. Conventional aluminum showed Ra = 41.1 nm, while chemical etching produced 3D

 doi:10.20944/preprints202509.1851.v1

micro/nano features with Ra = 169.4 nm, lateral size ~200 nm, and few nm heights [32]. These AFM-confirmed structures enhanced wettability, achieving a water contact angle of 167° [33-35], and significantly improved heat dissipation in heat sinks and heat pipes [36, 37]. On AA 6063, AFM-guided roughening initially increased corrosion resistance by up to two orders of magnitude [38, 39].

In a study on the microstructural, nanomechanical, and tribological properties of thin dense chromium coatings, AFM revealed a dense, nodular microstructure with 3.6 μm nodules and 227 nm grains [40]. SKPFM showed high surface potentials at nodule boundaries, which decreased post-NaCl exposure due to the formation of a stable Cr^{3+} oxide layer, as confirmed by X-ray Photoelectron Spectroscopy (XPS). The study on advanced nodular thin dense chromium coating with superior corrosion resistance reported a non-conductive bilayer oxide with a charge transfer resistance of 1.01 MΩ, significantly impeding Cl^- diffusion [41]. Statistical AFM quantified the microstructural contributions to corrosion resistance, demonstrating the coating's suitability for rolling bearing applications.

The study on the effect of phosphorous content on the microstructure and localized corrosion of electroless nickel-coated copper investigated NiP coatings with varying phosphorous (P) content (8.3–13.2 wt%) [42]. AFM revealed that high-P coatings (13.2 wt%) exhibited superior corrosion resistance due to their amorphous structure, while low-P coatings (8.3 wt%) showed localized corrosion at nodule boundaries. PSD and roughness analysis quantified microstructural effects, correlating crystallinity variations with electrochemical performance in 3.5% NaCl solution (Figure 6).

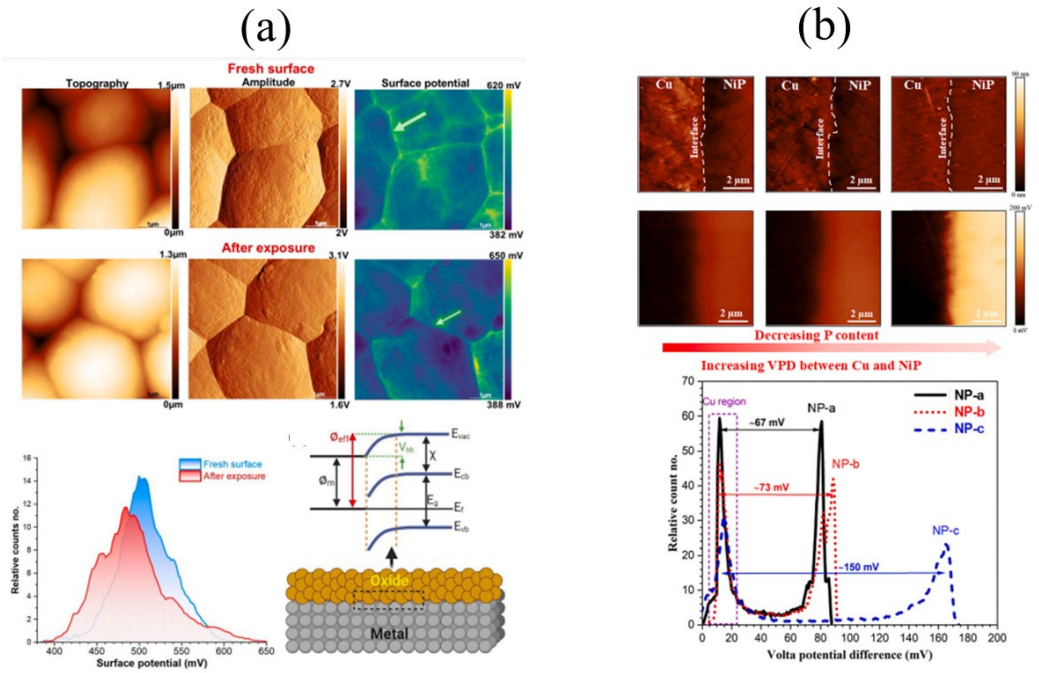

Figure 6. (a) Topography, amplitude, and surface potential maps of thin dense chromium (TDC) coatings, comparing a fresh surface with that exposed to 0.6 M NaCl solution for 7 days [43]. (b) Cross-sectional AFM morphology and SKPFM Volta potential maps for electroless nickel coatings with different phosphorus contents (NP-a, NP-b, NP-c), along with the histogram distribution of Volta potential differences across the cross-sections [42].

PSD and statistical roughness analysis offer detailed quantification of coating morphology across multiple spatial scales, enabling optimization of surface features for improved corrosion resistance, which goes well beyond the qualitative information provided by traditional line profiles. SKPFM plays a crucial role in detecting defect-driven galvanic cells, such as those at nodule

 doi:10.20944/preprints202509.1851.v1

boundaries, with nanoscale precision, facilitating targeted enhancements in coating durability under aggressive environmental conditions. Additionally, combining SKPFM with techniques like EIS, XPS, and SEM allows for a comprehensive correlation between electrochemical behavior, chemical composition, and surface potential variations, thereby improving the understanding of corrosion performance and inhibitor effectiveness.

3.4. Atmospheric and Localized Corrosion

Atmospheric and localized corrosion, driven by chloride-laden electrolytes or droplet-based exposure, are significant challenges in marine, aerospace, and industrial applications. These processes often involve dynamic electrochemical changes and pit initiation, which require real-time monitoring and nanoscale resolution to understand fully. In-situ SKPFM and statistical AFM techniques have enabled researchers to track transient corrosion phenomena, quantify environmental effects on corrosion kinetics, and predict pit initiation sites, providing critical insights for corrosion prevention.

A time-lapse SKPFM investigation on sensitized AA5083 aluminum alloy demonstrated that Mg_2Si particles undergo nobility inversion from cathodic to anodic behavior during chloride exposure in thin-film electrolytes at 20%–85% relative humidity [44]. Aluminides, both with and without silicon, functioned as dominant cathodic sites, while the surrounding alloy matrix in close proximity exhibited a shift in Volta potential toward that of the aluminides—a phenomenon referred to as "nobility adoption" (Figure 7). This reduced localized corrosion by altering anode/cathode ratios dynamically, as quantified by SKPFM's real-time potential mapping.

In a study about monitoring atmospheric corrosion under multi-droplet conditions, AFM combined with custom-designed electrical resistance (ER) sensors was used to quantify corrosion kinetics, enabling precise tracking of localized degradation [45]. Power-law droplet size distributions showed decreasing height and expanding width with progressive drying, with NaCl and surface roughness increasing corrosion rates. A strong correlation between corrosion rate and relative humidity was established using Savitzky-Golay filtering, highlighting the influence of droplet-based electrolyte conditions on corrosion kinetics.

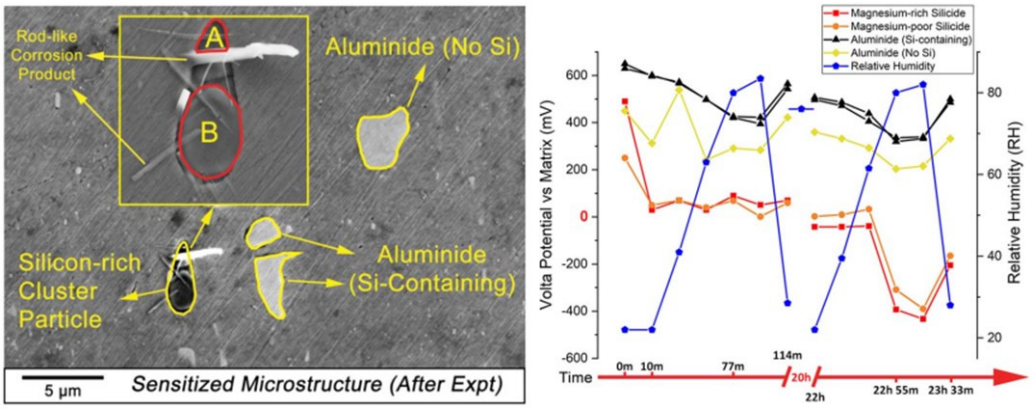

Figure 7. SEM image of the SKPFM scan region of the sensitized microstructure after corrosion experiments, with the inset showing a magnified view of a silicon-rich cluster particle. Regions A and B mark two distinct areas within the cluster. The Volta potential evolution of these particles is presented as a function of time during corrosion exposure, with the corresponding variation in relative humidity plotted alongside to highlight its influence on the potential changes [44].

In another study about atmospheric corrosion of iron under single droplets, AFM and a micro-sized three-electrode cell were employed to investigate the effects of droplet volume (1.5–5 µL) and NaCl concentration (0.01–0.2 M) on localized corrosion behavior [46]. Smaller droplets (1.5 µL) with higher NaCl concentrations exhibited lower noise resistance (R_n) and polarization resistance (R_p),

 doi:10.20944/preprints202509.1851.v1

enhancing localized corrosion due to chloride dominance over oxygen diffusion. Statistical AFM analysis provided topographic insights into droplet-induced corrosion, complementing electrochemical measurements.

In-situ SKPFM enables real-time electrochemical monitoring by capturing dynamic potential changes—such as nobility inversions—during corrosion processes, offering insights that static line profiles cannot provide. Additionally, statistical roughness analysis and power spectral density methods allow for quantitative assessment of corrosion kinetics, linking topographic evolution with environmental variables like relative humidity and chloride concentration. This integrated approach delivers a more comprehensive understanding of corrosion dynamics. Moreover, atomic force microscopy aids in predicting pit initiation by mapping variations in surface roughness and local electrochemical activity, thereby enabling predictive modeling of localized corrosion beyond the limitations of traditional, one-dimensional data.

3.5. Nanoparticles and Biointerfaces

Nanoparticles and biointerfaces—particularly in biomedical applications—are susceptible to corrosion and biodegradation, which are influenced by protein interactions and physiological environments. These interactions can affect nanoparticle stability, toxicity, and functionality, making their characterization critical for safe biomedical applications. AFM and SKPFM have been essential in quantifying electrochemical and morphological changes at the nanoscale, providing insights into protein-nanoparticle interactions and biodegradation mechanisms.

Rahimi et al. [47] investigated the biodegradation behavior of oxide nanoparticles in apoferritin protein media using a systematic electrochemical approach. SKPFM showed that a 5-nm bismuth ferrite (BFO) shell on cobalt ferrite (CFO) nanoparticles increased surface potential, reducing anodic current density and biodegradation rates. Potentiodynamic polarization measurements confirmed lower electrochemical activity in CFO-BFO due to higher flat band potential and lower donor density, highlighting the protective role of the BFO shell in protein-containing media.

In a study examining the physicochemical changes of apoferritin protein during the biodegradation of magnetic metal oxide nanoparticles, AFM and SKPFM were used to observe significant alterations during the degradation of $CoFe_2O_4$ nanoparticles [48]. Apoferritin's characteristic hole (1.35 nm) vanished after 48 hours, with protein height increasing from 3.5 to 7.5 nm due to hole filling by heterogeneous oxides (γ-Fe_2O_3, Fe_3O_4, CoO, etc.) (Figure 8). This led to a significant increase in surface potential, accelerating biodegradation through enhanced electrostatic interactions. Statistical analysis quantified these morphological and electrochemical changes, providing insights into nanoparticle toxicity and protein deformation.

Using AFM, researchers investigated the mechano-bactericidal properties of Psalmocharias cicada wings by quantifying nanopillar skewness and kurtosis on the wings of Psalmocharias querula (PQ) and P.akesensis (PA) [49]. PQ's nanopillars exhibited higher bactericidal efficiency due to effective bacterial membrane penetration, as confirmed by colony-forming unit (CFU) counts and AFM force measurements. PSD and histogram analysis correlated topographic features with antibacterial performance, offering insights into bioinspired surface design.

SKPFM offers nanoscale electrochemical mapping by quantifying interactions at nanoparticle–biointerface boundaries with high resolution, capturing protein-induced potential changes essential to understanding biodegradation—details that line profiles cannot reveal. AFM topography complements this by tracking nanoscale morphological evolution, such as protein hole filling or changes in nanopillar geometry, providing comprehensive insights into biointerface dynamics and nanoparticle stability. Additionally, statistical tools like power spectral density and histogram analysis enable quantitative assessment of both electrochemical and topographic variations, allowing precise correlation with biodegradation rates and toxicity, far exceeding the limited information available from traditional line profiles.

 doi:10.20944/preprints202509.1851.v1

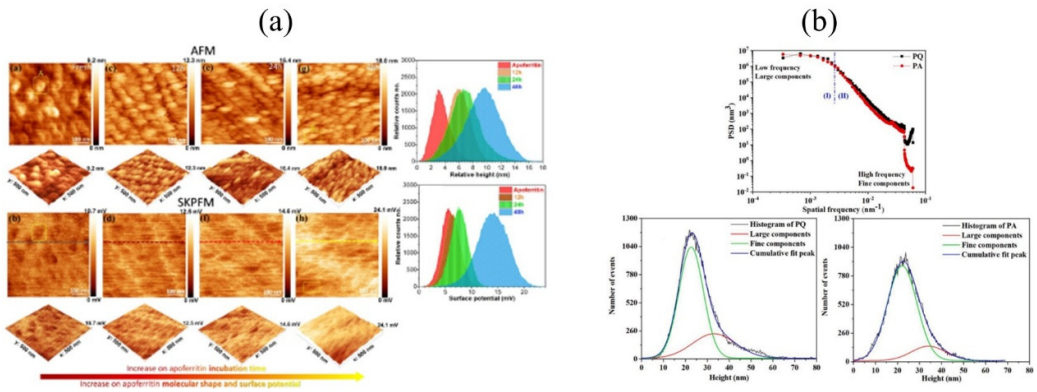

Figure 8. (a) 2D/3D AFM and SKPFM images showing the adsorption of apoferritin protein on oxide surfaces at different incubation times in the presence of CFO nanoparticles, along with height and surface potential histograms [48]. (b) AFM-based nanotopological analysis of cicada wings, including power spectral density graphs and histogram profiles of different wing regions (PQ and PA) [49].

3.6. Other Material Systems

Advanced AFM and SKPFM techniques have been applied to a diverse array of material systems, including nickel-aluminum bronze, aluminum alloys, martensitic stainless steels, and shape memory alloys. These studies highlight the versatility of these methods in addressing phase-specific corrosion, intergranular corrosion, and microstructural effects, providing a universal framework for corrosion analysis across industries like marine, aerospace, and biomedical engineering.

Nakhaie et al. [50] investigated the corrosion initiation behavior of NiAl bronze in acidic media, focusing on the role of its constituent phases using SEM–EDS, AFM, and SKPFM techniques. SKPFM mapped anodic iron-rich β phases and cathodic copper-rich α phases, correlating Volta potentials with theoretical work functions to confirm β phases as primary corrosion initiation sites. SEM and AFM imaging provided complementary topographic data, highlighting the influence of microstructural phase distribution on localized corrosion susceptibility.

Investigations into additively manufactured superelastic NiTi alloy revealed, through SKPFM analysis, that martensitic regions acted as anodic sites in laser powder bed fusion (LPBF) samples, highlighting the influence of crystallographic texture on corrosion resistance [51]. Optimizing LPBF parameters produced [001]-textured NiTi, eliminating martensite and reducing corrosion current by nearly two orders of magnitude, enhancing both corrosion resistance and superelastic performance (Figure 9).

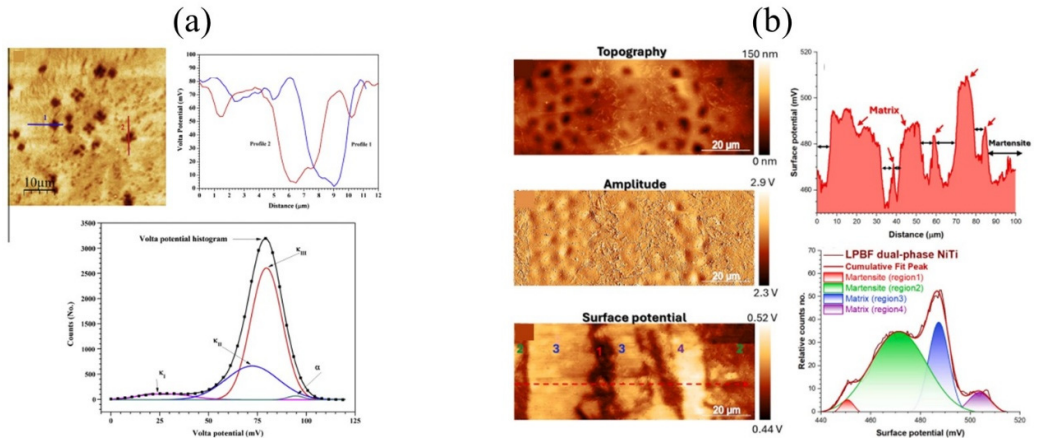

Figure 9. (a) Volta potential mapping of NiAl bronze, including line profiles and deconvoluted histogram of Gaussian distributions, where each peak corresponds to constituent phases [50]. (b) AFM topography,

 doi:10.20944/preprints202509.1851.v1

amplitude, and SKPFM mapping of LPBF dual-phase NiTi, along with Volta potential profiles and histogram analysis deconvoluted by Gaussian fitting [51].

4. Emerging Techniques and Advantages in Nanoscale Corrosion Analysis Using Advanced AFM

As discussed in Section 3, over the past decade, the evolution of advanced Atomic Force Microscopy techniques—such as Power Spectral Density analysis, Scanning Kelvin Probe Force Microscopy, multimodal Gaussian histogram evaluation, and statistical roughness quantification—has revolutionized the field of corrosion science. These methods have addressed the inherent limitations of traditional line profile analysis by providing spatially resolved, quantitative, and mechanistic insights at the nanoscale. Unlike conventional tools, these approaches can uncover early-stage corrosion phenomena by mapping surface heterogeneity, detecting micro-galvanic interactions, and capturing dynamic electrochemical behavior. Their effectiveness has been demonstrated across a wide array of materials, including aluminum-copper joints, NiAl bronze, dissimilar aluminum alloy welds (AA5083/AA7023), Ti-6Al-4V, duplex stainless steels, and superhydrophobic coatings. A major advancement in recent research has been the integration of in-situ AFM and SKPFM monitoring. This enables real-time imaging of corrosion events such as passive film breakdown, metastable pitting, and pit coalescence, particularly in chloride-rich environments. When combined with techniques like STEM-EDS, Mott-Schottky analysis, and SECM, these multimodal approaches yield comprehensive information that links microstructural, chemical, and electrochemical factors. For example, phase-specific corrosion activity in duplex stainless steels and intermetallic particle-driven degradation in aluminum alloys have been precisely characterized, offering a deeper understanding of material performance under corrosive conditions.

Additionally, the incorporation of machine learning and AI into AFM data analysis is facilitating high-throughput corrosion assessment. These tools can process complex datasets from PSD and SKPFM measurements to identify patterns, classify corrosion-prone features, and guide the development of predictive models for alloy design and surface treatments. Such automation enhances the accuracy and efficiency of corrosion diagnostics while promoting data-driven optimization strategies. Crucially, these methods provide phase-specific electrochemical mapping at nanometer resolution, identifying localized Volta potential differences around inclusions, precipitates, and secondary phases. This enables identification of corrosion hot spots that were previously undetectable. Statistical roughness metrics and PSD analysis offer quantifiable data that correlate microstructural features with corrosion susceptibility, thereby informing strategies for alloy development, protective coating design, and welding interface optimization. The broader applicability of these techniques extends across industries and materials, including aerospace-grade aluminum alloys, marine steels, biomedical implants, and responsive smart coatings. They inform strategies such as minimizing intermetallic particle size, engineering passive layer chemistry, or designing bioinspired superhydrophobic surfaces. Collectively, this advanced AFM-based framework offers not only a mechanistic understanding of corrosion but also actionable insights for enhancing material durability in increasingly demanding environments.

5. Outlook

A concise overview of representative studies that utilized AFM and complementary techniques to analyze surface properties and related performance in various material systems is summarized in Table 1. As can be seen, the scope of applications is expanding—from structural alloys and coatings to biomedical implants, additive manufacturing, and bioinspired surfaces—highlighting the versatility of these techniques. This convergence of nanoscale characterization, computational analytics, and emerging materials systems promises not only deeper mechanistic understanding but also predictive capabilities for designing corrosion-resistant materials in diverse industrial and biomedical contexts.

 doi:10.20944/preprints202509.1851.v1

Table 1. Summary of representative studies employing AFM and complementary techniques to investigate surface properties, structural features, and related performance across different material systems.

Alloy/Material System	Techniques Used	Analysis Methods	Main Outcomes	Reference	Year
Aluminum Alloys (EN AW-3003, AA5083/AA7023)	AFM, SKPFM, SECM	Line profile, Histogram, PSD, FFT	Corrosion at intermetallic particles; Volta potential mapping	[1-7]	2005-2011
Duplex Stainless Steel (2205)	SKPFM, EBSD	Line profile, Potential mapping	Strain-induced corrosion; ferrite vs austenite phases	[8, 9]	2015-2016
Super Duplex Stainless Steel	SKPFM, STEM-EDS, Mott-Schottky	Volta potential mapping, Statistical analysis	Ferrite nobler due to Mo/W/Cr; passive film heterogeneity	[10]	2019
FSW Al-Cu joints	SEM-EDS, AFM, SKPFM	Histograms, potential mapping	Micro-galvanic corrosion at IMC boundaries	[13]	2014
Ti-Cu Welded Bimetal	AFM, SKPFM	Histogram, FFT	Volta potential at Ti-Cu IMCs; nobility inversion after immersion	[16, 17]	2018
Low Alloy Steel A508/309L/308L Weld	AFM, SKPFM, SVET, SEM	PSD, Gaussian distribution, FFT	MnS inclusions as pit initiation; area ratio effects	[18]	2019
Ti-6Al-4V Alloy (Biomedical)	AFM, SKPFM, Mott-Schottky	Histogram, PSD	Cold work raises passive current; α-phase anodic	[20]	2015
CoCrMo Implant Alloy	SKPFM, SEM, Mott-Schottky	Histogram, Roughness quantification	Protein adsorption lowers Volta potential; accelerates corrosion	[23]	2022
WE43 Mg Alloy	AFM, SKPFM, SEM	Statistical roughness analysis	Protein-electrolyte effects on Mg degradation	[24]	2024
Ni Superhydrophobic Coatings	AFM, SKPFM, SEM-EDS, EIS	PSD, Histogram	Surface roughness enhances hydrophobicity & corrosion resistance	[26]	2018
Thin Dense Chromium (TDC) Coatings	AFM, SKPFM, XPS	Histogram, PSD	Nodule boundaries active; stable Cr oxide protective	[40]	2024
Electroless Ni-P Coatings	AFM, SKPFM	PSD, Roughness analysis	High-P amorphous NiP improves resistance; low-P localized corrosion	[42]	2024
NiAl Bronze	AFM, SKPFM, SEM-EDS	Histogram, Line profile	β-phase anodic, α-phase cathodic; phase-specific initiation	[50]	2014
Nanoparticles (CFO, BFO shells)	AFM, SKPFM, Electrochemistry	Histogram, Statistical analysis	BFO shell reduces nanoparticle corrosion in protein media	[47]	2023
NiTi Shape Memory Alloy (Additive Manufacturing)	SKPFM	Histogram, Potential mapping	Martensite anodic; [001]-textured NiTi more resistant	[51]	2025
Cicada Wings (Biointerfaces)	AFM	PSD, Histogram	Nanopillar geometry controls bactericidal efficiency	[49]	2021

As the field advances, the integration of AFM with spectroscopy, electrochemistry, and machine learning holds transformative potential for corrosion science. Key future directions include:

 doi:10.20944/preprints202509.1851.v1

- *Multimodal Integration:* Correlative techniques such as Raman-AFM, SECM-AFM, and EIS-AFM will enhance chemical and electrochemical characterization alongside morphological mapping.
- *Machine Learning and Automation for data analysis:* AI-driven feature recognition, classification, and predictive modeling will streamline large-scale data analysis, enabling faster and more accurate insights.
- *High-Speed and* In-Situ *Techniques:* Real-time AFM imaging with high temporal resolution will allow the capture of transient corrosion phenomena, advancing kinetic understanding.
- *Standardization of Statistical Protocols:* Establishing universal methods for PSD, roughness quantification, and multimodal Gaussian analysis will improve reproducibility and allow cross-laboratory and cross-material comparisons.
- *Long-Term and Real-World Relevance:* In-situ AFM studies in realistic service environments will bridge the gap between short-term experiments and long-term durability, enhancing industrial applicability.

6. Conclusions

This review has outlined recent advances in nanoscale corrosion characterization using AFM-based techniques and their integration with complementary methods, highlighting both the scientific insights gained and the challenges that remain.

This review has critically evaluated the transformative role of advanced AFM and SKPFM techniques in unraveling nanoscale corrosion phenomena. By moving beyond conventional line profile analysis, we highlighted how power spectral density (PSD), multimodal Gaussian fitting, statistical roughness quantification, and deconvolution approaches offer quantitative and spatially resolved insights into corrosion initiation, propagation, and microstructural influences. These methods have proven effective across diverse material systems, including dissimilar welds, biomedical implants, protective coatings, and nanoparticle–biointerfaces. Their integration with complementary techniques such as SEM-EDS, SECM, Mott-Schottky analysis, and in-situ electrochemical methods enables a comprehensive, multi-modal understanding of localized corrosion mechanisms.

Advantages of results evaluation beyond line profiles in AFM & SKPFM for corrosion studies as summarized as below:

- **Comprehensive mapping:** Full 2D and 3D evaluation of AFM and SKPFM images provides complete coverage of surface roughness and potential variations that cannot be captured by single line profiles.
- **Scale-resolved insights:** Spectral analysis enables the separation of fine-scale and coarse-scale corrosion features, offering a clearer understanding of different degradation mechanisms.
- **Quantitative statistics:** Population-based statistical analysis allows distinct identification and quantification of phases, oxides, and corrosion products within the scanned area.
- **Improved accuracy:** Deconvolution techniques correct tip-induced artefacts, yielding truer representations of both morphology and local potential distributions.
- **Dynamic tracking:** Time-lapse AFM and SKPFM imaging captures the evolution of transient corrosion processes, providing kinetic information at the nanoscale.
- **Mechanistic depth:** Integration with complementary methods links structural, chemical, and electrochemical information, enabling a more comprehensive understanding of corrosion mechanisms.

Importantly, this review underscores that advanced AFM-based analysis is not just a diagnostic tool but a predictive platform for corrosion science—capable of identifying electrochemical hot spots, evaluating the stability of passive films, and guiding the design of corrosion-resistant materials. As the field evolves, the convergence of in-situ AFM imaging, machine learning, and high-throughput data analysis will drive the next generation of corrosion diagnostics and materials development. The

 doi:10.20944/preprints202509.1851.v1

continued refinement and standardization of these approaches will be essential for ensuring reproducibility, cross-platform compatibility, and broader industrial application.

Author Contributions: All authors contributed to the conceptualization, writing, review, and editing of the manuscript. All authors have read and approved the final version for publication. *Artificial intelligence tools were used solely for grammar and linguistic refinement; all scientific content, analysis, and interpretations were prepared by the authors*.

Funding: This research received no external funding.

Acknowledgments: This work draws inspiration from the distinguished legacy of corrosion research at Royal Institute of Technology, KTH. We gratefully acknowledge the invaluable mentorship and scientific leadership of Professor Christofer Leygraf and Professor Jinshan Pan, whose pioneering contributions laid the foundation for nanoscale corrosion analysis. AD also extends his sincere thanks to KTH, Ferdowsi University of Mashhad (FUM), and Hakim Sabzevari University (HSU) for their continuous support during his Ph.D. and subsequent research as a faculty member, as well as to all students who contributed during his tenure. Special appreciation is given for the advanced AFM and SKPFM facilities provided, which were instrumental in enabling this research.

Conflicts of Interest: The authors declare no conflicts of interest.

References

1. Davoodi A, Pan J, Leygraf C, Norgren S (2005) In Situ Investigation of Localized Corrosion of Aluminum Alloys in Chloride Solution Using Integrated EC-AFM/SECM Techniques. Electrochemical and Solid-State Letters 8:B21. 10.1149/1.1911900
2. Davoodi A, Pan J, Leygraf C, Norgren S (2006) Probing of local dissolution of Al-alloys in chloride solutions by AFM and SECM. Applied Surface Science 252:5499-5503. https://doi.org/10.1016/j.apsusc.2005.12.023
3. Davoodi A, Pan J, Leygraf C, Norgren S (2007) Integrated AFM and SECM for in situ studies of localized corrosion of Al alloys. Electrochimica Acta 52:7697-7705. https://doi.org/10.1016/j.electacta.2006.12.073
4. Davoodi A, Pan J, Leygraf C, Norgren S (2008) The Role of Intermetallic Particles in Localized Corrosion of an Aluminum Alloy Studied by SKPFM and Integrated AFM/SECM. Journal of The Electrochemical Society 155:C211. 10.1149/1.2883737
5. Davoodi A, Pan J, Leygraf C, Norgren S (2008) Multianalytical and In Situ Studies of Localized Corrosion of EN AW-3003 Alloy—Influence of Intermetallic Particles. Journal of The Electrochemical Society 155:C138. 10.1149/1.2834454
6. Davoodi A, Farzadi A, Pan J, Leygraf C, Zhu Y (2008) Developing an AFM-Based SECM System; Instrumental Setup, SECM Simulation, Characterization, and Calibration. Journal of The Electrochemical Society 155:C474. 10.1149/1.2943324
7. Davoodi A, Pan J, Leygraf C, Parvizi R (2011) Minuscule device for hydrogen generation/electrical energy collection system on aluminum alloy surface. International Journal of Hydrogen Energy 36:2855-2859. https://doi.org/10.1016/j.ijhydene.2010.11.048
8. Örnek C, Engelberg DL (2015) SKPFM measured Volta potential correlated with strain localisation in microstructure to understand corrosion susceptibility of cold-rolled grade 2205 duplex stainless steel. Corrosion Science 99:164-171. https://doi.org/10.1016/j.corsci.2015.06.035
9. Örnek C, Engelberg DL (2016) Correlative EBSD and SKPFM characterisation of microstructure development to assist determination of corrosion propensity in grade 2205 duplex stainless steel. Journal of Materials Science 51:1931-1948. 10.1007/s10853-015-9501-3
10. Rahimi E, Kosari A, Hosseinpour S, Davoodi A, Zandbergen H, Mol JMC (2019) Characterization of the passive layer on ferrite and austenite phases of super duplex stainless steel. Applied Surface Science 496:143634. https://doi.org/10.1016/j.apsusc.2019.143634
11. Bartawi EH, Marioara CD, Shaban G, Rahimi E, Mishin OV, Sunde JK, Gonzalez-Garcia Y, Holmestad R, Ambat R (2024) Effects of grain boundary chemistry and precipitate structure on intergranular corrosion

 doi:10.20944/preprints202509.1851.v1

in Al-Mg-Si alloys doped with Cu and Zn. Corrosion Science 236:112227. https://doi.org/10.1016/j.corsci.2024.112227

12. Li G, Li Z, Rahimi E, Muratori M, Smith A, Navarro MJS, Gonzalez-Garcia Y (2024) Pit initiation in quenching and partitioning processed martensitic stainless steels. Electrochimica Acta 498:144646. https://doi.org/10.1016/j.electacta.2024.144646
13. Sarvghad-Moghaddam M, Parvizi R, Davoodi A, Haddad-Sabzevar M, Imani A (2014) Establishing a correlation between interfacial microstructures and corrosion initiation sites in Al/Cu joints by SEM–EDS and AFM–SKPFM. Corrosion Science 79:148-158. https://doi.org/10.1016/j.corsci.2013.10.039
14. Davoodi A, Esfahani Z, Sarvghad M (2016) Microstructure and corrosion characterization of the interfacial region in dissimilar friction stir welded AA5083 to AA7023. Corrosion Science 107:133-144. https://doi.org/10.1016/j.corsci.2016.02.027
15. Esfahani Z, Rahimi E, Sarvghad M, Rafsanjani-Abbasi A, Davoodi A (2018) Correlation between the histogram and power spectral density analysis of AFM and SKPFM images in an AA7023/AA5083 FSW joint. Journal of Alloys and Compounds 744:174-181. https://doi.org/10.1016/j.jallcom.2018.02.106
16. Rahimi E, Rafsanjani-Abbasi A, Imani A, Hosseinpour S, Davoodi A (2018) Correlation of surface Volta potential with galvanic corrosion initiation sites in solid-state welded Ti-Cu bimetal using AFM-SKPFM. Corrosion Science 140:30-39. https://doi.org/10.1016/j.corsci.2018.06.026
17. Rahimi E, Rafsanjani-Abbasi A, Imani A, Hosseinpour S, Davoodi A (2018) Insights into Galvanic Corrosion Behavior of Ti-Cu Dissimilar Joint: Effect of Microstructure and Volta Potential. 11:
18. Okonkwo BO, Ming H, Zhang Z, Wang J, Rahimi E, Hosseinpour S, Davoodi A (2019) Microscale investigation of the correlation between microstructure and galvanic corrosion of low alloy steel A508 and its welded 309/308L stainless steel overlayer. Corrosion Science 154:49-60. https://doi.org/10.1016/j.corsci.2019.03.027
19. Okonkwo BO, Ming H, Wang J, Han E-H, Rahimi E, Davoodi A, Hosseinpour S (2021) A new method to determine the synergistic effects of area ratio and microstructure on the galvanic corrosion of LAS A508/309 L/308 L SS dissimilar metals weld. Journal of Materials Science & Technology 78:38-50. https://doi.org/10.1016/j.jmst.2020.10.044
20. Nakhaie D, Davoodi A, Ebrahimi GR (2015) The Influence of Cold Plastic Deformation on Passivity of Ti-6Al-4V Alloy Studied by Electrochemical and Local Probing Techniques. Corrosion 72:110-118. 10.5006/1794
21. Rahimi E, Offoiach R, Hosseinpour S, Davoodi A, Baert K, Lutz A, Terryn H, Lekka M, Fedrizzi L (2021) Effect of hydrogen peroxide on bovine serum albumin adsorption on Ti6Al4V alloy: A scanning Kelvin probe force microscopy study. Applied Surface Science 563:150364. https://doi.org/10.1016/j.apsusc.2021.150364
22. Rahimi E, Offoiach R, Deng S, Chen X, Pané S, Fedrizzi L, Lekka M (2021) Corrosion mechanisms of magnetic microrobotic platforms in protein media. Applied Materials Today 24:101135. https://doi.org/10.1016/j.apmt.2021.101135
23. Rahimi E, Offoiach R, Baert K, Terryn H, Fedrizzi L, Lekka M (2022) Albumin Protein Adsorption on CoCrMo Implant Alloy: Impact on the Corrosion Behaviour at Localized Scale. Journal of The Electrochemical Society 169:031507. 10.1149/1945-7111/ac5a1b
24. Imani A, Rahimi E, Lekka M, Andreatta F, Magnan M, Gonzalez-Garcia Y, Mol A, Raman RKS, Fedrizzi L, Asselin E (2024) Albumin Protein Impact on Early-Stage In Vitro Biodegradation of Magnesium Alloy (WE43). ACS Applied Materials & Interfaces 16:1659-1674. 10.1021/acsami.3c12381
25. Rahimi E, Imani A, Lekka M, Andreatta F, Gonzalez-Garcia Y, Mol JMC, Asselin E, Fedrizzi L (2022) Morphological and Surface Potential Characterization of Protein Nanobiofilm Formation on Magnesium Alloy Oxide: Their Role in Biodegradation. Langmuir 38:10854-10866. 10.1021/acs.langmuir.2c01540
26. Rahimi E, Rafsanjani-Abbasi A, Kiani-Rashid A, Jafari H, Davoodi A (2018) Morphology modification of electrodeposited superhydrophobic nickel coating for enhanced corrosion performance studied by AFM, SEM-EDS and electrochemical measurements. Colloids and Surfaces A: Physicochemical and Engineering Aspects 547:81-94. https://doi.org/10.1016/j.colsurfa.2018.03.045

 doi:10.20944/preprints202509.1851.v1

27. Rahimi E, Davoodi A, Kiani Rashid AR (2018) Characterization of screw dislocation-driven growth in nickel micro-nanostructure electrodeposition process by AFM. Materials Letters 210:341-344. https://doi.org/10.1016/j.matlet.2017.09.057
28. Rahimi E, Rafsanjani-Abbasi A, Davoodi A, Kiani-Rashid A (2018) Shape evolution of water and saline droplets during icing/melting cycles on superhydrophobic surface. Surface and Coatings Technology 333:201-209. https://doi.org/10.1016/j.surfcoat.2017.10.083
29. Noorbakhsh Nezhad AH, Davoodi A, Mohammadi Zahrani E, Arefinia R (2020) The effects of an inorganic corrosion inhibitor on the electrochemical behavior of superhydrophobic micro-nano structured Ni films in 3.5% NaCl solution. Surface and Coatings Technology 395:125946. https://doi.org/10.1016/j.surfcoat.2020.125946
30. Attar MR, Kazemi M, Salami B, Noori H, Passandideh-Fard M, Hosseinpour S, Davoodi A, Mohammadi M (2023) Improving Thermal Management of CPU by Surface Roughening of Heat Sinks. Arabian Journal for Science and Engineering 49:2153-2164. https://doi.org/10.1007/s13369-023-08182-0
31. Attar MR (2021) Creating Roughness on the Surface of 6000 Series Aluminum Alloy by Chemical Etching Method and Investigating its Superhydrophobic Properties and Heat Transfer. Dissertation, Ferdowsi University of Mashhad
32. Attar MR, Mohammadi M, Taheri A, Hosseinpour S, Passandideh-Fard M, Haddad Sabzevar M, Davoodi A (2020) Heat transfer enhancement of conventional aluminum heat sinks with an innovative, cost-effective, and simple chemical roughening method. Thermal Science and Engineering Progress 20:100742-100752. https://doi.org/10.1016/j.tsep.2020.100742
33. Attar MR, Davoodi A: A Novel Process to Fabricate Superhydrophobic Nano-structured Surface on Aluminum Alloy by Simple Immersion Etching Method; in 6th International Conference of Materials Engineering and Metallurgy (iMAT). Tehran, Iran, 2017
34. Attar MR, Khajavian E, Hosseinpour S, Davoodi A (2019) Fabrication of micro–nano-roughened surface with superhydrophobic character on an aluminium alloy surface by a facile chemical etching process. Bulletin of Materials Science 43:31-39. https://doi.org/10.1007/s12034-019-1998-7
35. Attar MR, Darband GB, Davoodi A: Evaporative Cooling through Superhydrophilic Surface Structuring for Thermal Management; in The First International Conference on Applied Research in Engineering. Melbourne, Australia, 2025
36. Ghazi T, Attar MR, Ghorbani A, Alshihmani H, Davoodi A, Passandideh-Fard M, Sardarabadi M (2023) Synergistic effect of active-passive methods using fins surface roughness and fluid flow for improving cooling performance of heat sink heat pipes. Experimental Heat Transfer 37:649-664. https://doi.org/10.1080/08916152.2023.2182838
37. Attar MR: Greener Computing: Faster Data Processing with Lower Environmental Impact; in 1st Khwarizmi International Conference on Science and Technology. Tehran, Iran, 2024
38. Khajavian E, Attar MR, Mohammadi Zahrani E, Liu W, Davoodi A, Hosseinpour S (2022) Tuning surface wettability of aluminum surface and its correlation with short and long term corrosion resistance in saline solutions. Surface and Coatings Technology 429:127950-127963. https://doi.org/10.1016/j.surfcoat.2021.127950
39. Attar M, Eskandariyoon FP, Davodi A, Khajavian E, Taji I: The Effect of the Chromate Inhibitor on the Aluminium Alloy Superhydrophobic Surfaces; in 5th Iran International Aluminium Conference & Exhibition (IIAC). Tehran, Iran, 2018
40. Broitman E, Jahagirdar A, Rahimi E, Meeuwenoord R, Mol JMC (2024) Microstructural, Nanomechanical, and Tribological Properties of Thin Dense Chromium Coatings. 14:
41. Rahimi E, Nijdam T, Jahagirdar A, Broitman E, Mol A (2025) Advanced Nodular Thin Dense Chromium Coating: Superior Corrosion Resistance. ACS Applied Materials & Interfaces 17:8588-8600. 10.1021/acsami.4c19897
42. Mousavi M, Rahimi E, Mol JMC, Gonzalez-Garcia Y (2024) The effect of phosphorous content on the microstructure and localised corrosion of electroless nickel-coated copper. Surface and Coatings Technology 492:131174. https://doi.org/10.1016/j.surfcoat.2024.131174

 doi:10.20944/preprints202509.1851.v1

43. Rahimi E, Nijdam T, Jahagirdar A, Broitman E, Mol A (2025) Improved surface charge and corrosion resistance at the near-nanocrystalline chromium/nano-bilayer oxide interface in advanced thin dense chromium coatings. Applied Surface Science 689:162504. https://doi.org/10.1016/j.apsusc.2025.162504
44. Liew Y, Örnek C, Pan J, Thierry D, Wijesinghe S, Blackwood DJ (2020) In-Situ Time-Lapse SKPFM Investigation of Sensitized AA5083 Aluminum Alloy to Understand Localized Corrosion. Journal of The Electrochemical Society 167:141502. 10.1149/1945-7111/abc30d
45. Zhang K, Rahimi E, Van den Steen N, Terryn H, Mol A, Gonzalez-Garcia Y (2024) Monitoring atmospheric corrosion under multi-droplet conditions by electrical resistance sensor measurement. Corrosion Science 236:112271. https://doi.org/10.1016/j.corsci.2024.112271
46. Rahimi E, Zhang K, Kosari A, Van den Steen N, Homborg A, Terryn H, Mol A, Gonzalez-Garcia Y (2024) Atmospheric corrosion of iron under a single droplet: A new systematic multi-electrochemical approach. Corrosion Science 235:112171. https://doi.org/10.1016/j.corsci.2024.112171
47. Rahimi E, Kim D, Offoiach R, Sanchis-Gual R, Chen X-Z, Taheri P, Gonzalez-Garcia Y, Mol JMC, Fedrizzi L, Pané S, Lekka M (2023) Biodegradation of Oxide Nanoparticles in Apoferritin Protein Media: A Systematic Electrochemical Approach. Advanced Materials Interfaces 10:2300558. https://doi.org/10.1002/admi.202300558
48. Rahimi E, Imani A, Kim D, Rahimi M, Fedrizzi L, Mol A, Asselin E, Pané S, Lekka M (2024) Physicochemical Changes of Apoferritin Protein during Biodegradation of Magnetic Metal Oxide Nanoparticles. ACS Applied Materials & Interfaces 16:53299-53310. 10.1021/acsami.4c12269
49. Dehghani S, Mashreghi M, Nezhad AHN, Karimi J, Hosseinpour S, Davoodi A (2021) Exploring mechano-bactericidal nature of Psalmocharias cicadas wings: an analytical nanotopology investigation based on atomic force microscopy characterization. Surfaces and Interfaces 26:101407. https://doi.org/10.1016/j.surfin.2021.101407
50. Nakhaie D, Davoodi A, Imani A (2014) The role of constituent phases on corrosion initiation of NiAl bronze in acidic media studied by SEM–EDS, AFM and SKPFM. Corrosion Science 80:104-110. https://doi.org/10.1016/j.corsci.2013.11.017
51. Zhu J-N, Li Z, Rahimi E, Yan Z, Ding Z, Mol A, Popovich V (2025) Enhancing corrosion resistance through crystallographic texture control in additively manufactured superelastic NiTi alloy. Corrosion Science 251:112929. https://doi.org/10.1016/j.corsci.2025.112929